ResearchGate

See discussions, stats, and author profiles for this publication at: https://www.researchgate.net/publication/312551611

Physics based Modeling of Gate Current including Fowler-Nordheim Tunneling in GaN HEMT

Conference Paper · December 2016

CITATIONS
0

READS
20

5 authors, including:

Sudip Ghosh
Indian Institute of Technology Kanpur
22 PUBLICATIONS 13 CITATIONS

SEE PROFILE

Avirup Dasgupta
Indian Institute of Technology Kanpur
26 PUBLICATIONS 19 CITATIONS

SEE PROFILE

Sourabh Khandelwal
University of California, Berkeley
99 PUBLICATIONS 283 CITATIONS

SEE PROFILE

Yogesh Singh Chauhan
Indian Institute of Technology Kanpur
161 PUBLICATIONS 484 CITATIONS

SEE PROFILE

Some of the authors of this publication are also working on these related projects:

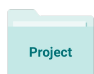

Modeling and simulation of III-V and Ge transistors for logic and power applications View project

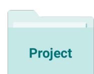

Modeling Advanced FDSOI for IC Design View project

All content following this page was uploaded by Yogesh Singh Chauhan on 20 January 2017.

The user has requested enhancement of the downloaded file.

Physics based Modeling of Gate Current including Fowler-Nordheim Tunneling in GaN HEMT

Sudip Ghosh, Avirup Dasgupta,
Aloke K. Dutta, and Yogesh Singh Chauhan
Nanolab, Dept. of Electrical Engineering,
Indian Institute of Technology Kanpur, India
Email: sudip@iitk.ac.in, chauhan@iitk.ac.in

Sourabh Khandelwal
Dept. of Electrical Engineering and Computer Science,
University of California Berkeley, USA

***Abstract*—In this paper, we report the major conduction mechanisms of the gate leakage current (I_g) in AlGaN/GaN HEMTs and develop an analytical model for it in a surface-potential based framework. GaN HEMTs with higher Al mole fraction in the AlGaN barrier layer experiences high electric field across this layer in the strong reverse gate bias region, leading to a significant Fowler-Nordheim (FN) tunneling current. Accurate modeling of the FN tunneling component is very important for this device along with the Poole-Frenkel (PF) emission current which dominates in relatively lower negative bias. We have demonstrated that the electric field across the barrier layer does not saturate even in very high reverse gate bias and is sufficient to increase reverse gate leakage current drastically by the FN tunneling process. Thermionic emission (TE) mechanism plays a major role in determining the forward gate current, whereas trap-assisted tunneling (TAT) current acts in the vicinity of zero gate bias. In this work, these components have been modeled and validated with the experimental data for a wide range of bias and temperature, demonstrating the weak and strong temperature dependence of FN and PF components, respectively.**

***Index Terms*—GaN HEMT, Gate Leakage Current, Fowler-Nordheim Tunneling, Poole-Frenkel Emission, Compact Model.**

I. Introduction

AlGaN/GaN HEMTs have many attractive properties such as high breakdown voltage, high 2-DEG charge density and high electron mobility, which make it a suitable candidate for the high power as well as high frequency applications [1], [2]. Despite all these advantages, excessive reverse gate leakage current is a limiting factor [3–5] in these devices and a topic of research interest. High gate leakage current may significantly reduce the breakdown voltage and increase the noise figure [6]. Leakage of electrons from gate material is also responsible for surface state trapping related current collapse phenomenon observed in GaN HEMTs [7].

Recent studies [8], [9] show higher Al mole fraction in AlGaN layer results in higher drain current density but at the cost of increasing FN tunneling current due to the introduction of high electric field across the barrier layer. This FN tunneling current becomes pronounced even at room temperature and above, and the inclusion of this component is immensely important for the accurate modeling of the gate current. In this work, we derive an analytical model for the total FN tunneling current from its current density expression, which is a function of electric field. This electric-field is calculated in terms of surface potential (ψ), obtained in our surface potential (SP) based GaN HEMT compact model named Advanced Spice Model for High Electron Mobility Transistor (ASM-HEMT) [10–14].

Although it has been reported [8], [9], [15] that the electric field across the barrier layer saturates beyond the threshold voltage (V_{OFF}), and hence, field dependent reverse gate leakage current saturates in this region, we demonstrate that the electric field gradually increases at a slower rate even beyond V_{OFF}, resulting in a drastic increase of the reverse gate leakage current, which could be clearly observed through the measured gate current plots in linear scale. This effect is captured in this work through modified field calculation, which is necessary for the GaN HEMT circuit design, operating in the high negative gate bias region.

In our earlier work [13], we presented the model of gate current which consists of three components; PF, TAT (in low-to-medium reverse bias region) and TE (forward bias region). This paper presents improved current expressions for these three components, which are computationally more efficient and have better convergence for a wide bias range compared to the earlier model. The complete gate current model is implemented in ASM-HEMT Verilog-A model code, which is under consideration for standardization at the Compact Model Coalition (CMC) [16].

II. Gate Current Model Description

A. Fowler-Nordheim Tunneling Model

High reverse gate voltage increases the electric field across the AlGaN barrier layer, which in turn reduces the thickness of the barrier at the metal Fermi level. Electrons from gate metal can easily tunnel across this thin triangular barrier, adding FN tunneling current (see Fig. 1). AlGaN/GaN devices with higher Al mole fraction introduces more electric field across the barrier resulting in more FN tunneling current in this bias range. This tunneling process is independent of temperature and should be clearly visible at low temperature, where PF emission current is low. However, for devices with higher Al mole fraction, this FN component has significant role in determining the reverse gate leakage current, even at room temperature or above.

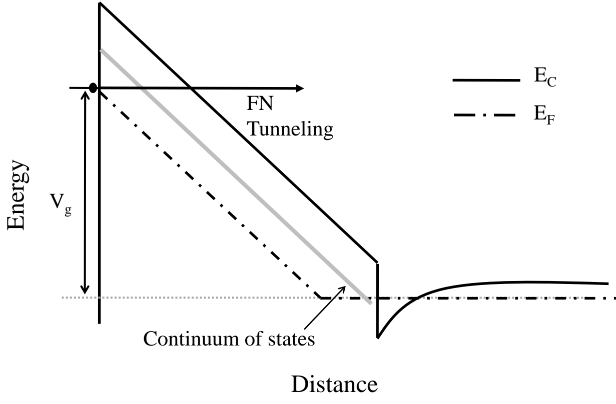

Fig. 1: Conduction band diagram of AlGaN/GaN HEMT in high reverse gate voltage shows the FN tunneling mechanism. High electric field reduces the thickness of the barrier at the metal Fermi level, and from gate metal electron can easily tunnel across this thin triangular barrier, resulting in FN current.

The FN tunneling current density (J_{FN}) can be expressed as [9], [15]:

$$J_{FN} = A \cdot E^2 \cdot exp\left(\frac{-B}{E}\right) \quad (1)$$

where $B = 8\pi\sqrt{2m_n^*(q\phi_{eff})^3}/3qh$, A is a constant, E is the electric field across the AlGaN barrier layer, m_n^* is the effective mass of electron in semiconductor, ϕ_{eff} is the effective barrier height, and h is the Planck's constant. The electric field at the metal-AlGaN layer is calculated as:

$$E = \frac{q\sigma_p - C_g(V_{go} - \psi)}{\epsilon_s} \quad (2)$$

where σ_P is the sum of the piezoelectric polarization charge in the barrier and the difference between spontaneous polarization charge in the barrier and the buffer, C_g is the gate capacitance, q the electron charge, and V_{go} is the difference between applied gate voltage and V_{OFF}. To obtain the total current, we have to integrate the current density along the channel length from source to the drain.

$$I_{FN} = W\int_0^L J_{FN} \cdot dx \quad (3)$$

To integrate, we change the integration variable from x to ψ using the expression [10]:

$$\frac{dx}{d\psi} = \frac{L\,(V_{g0} - \psi + V_{th})}{(V_{g0} - \psi_m + V_{th})\,(\psi_d - \psi_s)} = L \cdot \frac{(K - s)}{K \cdot \Delta\psi} \quad (4)$$

where ψ_s, ψ_d, and ψ_m are source side, drain side and average surface potential, respectively, $K = (V_{g0} - \psi_m + V_{th})$, $s = \psi - \psi_m$, $\Delta\psi = \psi_d - \psi_s$, and L is the channel length. Now we can change the integral variable $dx \rightarrow d\psi \rightarrow ds$ and the limits $0 \rightarrow \psi_s \rightarrow -\Delta\psi/2$, and $L \rightarrow \psi_d \rightarrow +\Delta\psi/2$. Equation (3) can be written as:

$$I_{FN} = \frac{WLA}{K\Delta\psi}\int_{-\Delta\psi/2}^{\Delta\psi/2} E^2 \cdot (K - s) \cdot exp\left(\frac{-B}{E}\right) \cdot ds \quad (5)$$

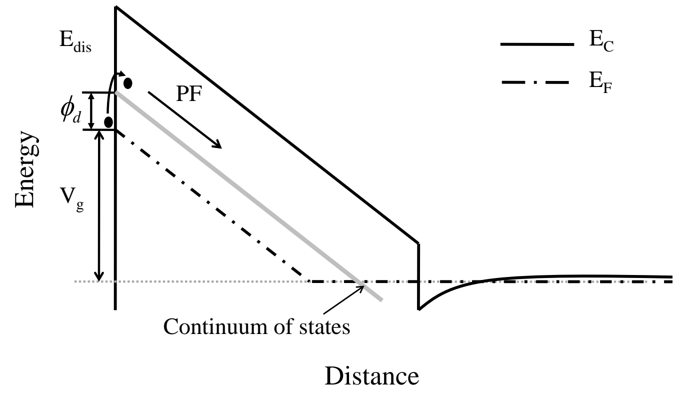

Fig. 2: Conduction band edge diagram of AlGaN/GaN HEMT for medium reverse gate voltage showing the electric field-enhanced thermal emission of electrons from a trap state to the continuum states associated with a conductive dislocation. Continuum of states (E_{dis}, marked in gray) is at a height ϕ_d from the metal Fermi level. The trap states in the barrier are assumed to be very close to the metal Fermi level.

Before performing the integration appearing in (5), the inverse of the electric field term in the exponential is approximated by the Taylor series expansion around the average surface potential ψ_m, which results into a compact form of solution. So the electric field and its inverse can be expressed as $E = E_m + s/d$ and $1/E = 1/E_m - s/(E_m^2 \cdot d)$, respectively. where E_m is the electric field calculated at $\psi = \psi_m$, and d is the thickness of the barrier layer. Now substituting these electric field terms in Eq. (5) and performing the integration, we can obtain the final expression of the total FN tunneling current as:

$$\begin{aligned} I_{FN} =& K' \Bigg[\left(\frac{K_1}{K_5} - \frac{K_2}{K_5^2} + \frac{2K_3}{K_5^3} - \frac{6K_4}{K_5^4}\right) \frac{sinh\,(K_5\Delta\psi/2)}{\Delta\psi/2} \\ &+ \Delta\psi/2\left(\frac{K_3}{K_5} - \frac{3K_4}{K_5^2}\right) sinh\left(\frac{K_5\Delta\psi}{2}\right) \\ &+ \left(\frac{K_2}{K_5} - \frac{2K_3}{K_5^3} + \frac{6K_4}{K_5^3} + \frac{K_4}{K_5} \cdot \frac{\Delta\psi^2}{4}\right) cosh\left(\frac{K_5\Delta\psi}{2}\right) \Bigg] \end{aligned} \quad (6)$$

where the variables are assigned as; $K' = (WLA/K)exp(-B/E_m)$, $K_1 = KE_m^2$, $K_2 = 2E_mK/d - E_m^2$, $K_3 = K/d^2 - 2E_m/d$, $K_4 = -1/d^2$, and $K_5 = B/(E_m^2 d)$.

For the sake of simplicity, we have used 60:40 partitioning scheme to the source and drain terminal, respectively.

B. Poole-Frenkel and Trap-Assisted Tunneling Components

Under low to medium negative V_g bias region, the reverse gate leakage current is dominated by the PF emission and the TAT mechanisms. PF emission is the electric field-enhanced thermal emission of electrons from a trap state to the continuum states associated with a conductive dislocation [3–5], [15]. Typical conduction band diagram at a medium applied gate bias is shown in Fig. 2 describing this mechanism, where the continuum of states (E_{dis}, marked in gray) is at a height ϕ_d from the metal Fermi level. The trap states in the barrier

are assumed to be very close to the metal Fermi level, from where electrons can transport through the continuum of states to the GaN 2-DEG layer by gaining thermal energy. The PF conduction has a strong temperature dependence.

The relation between the current density (J_{PF}) and the electric field (E) for PF conduction is given by [17]:

$$J_{PF} = C \cdot E \cdot exp(\alpha + \beta\sqrt{E}) \tag{7}$$

where $\alpha = -\phi_d/V_{th}$ and $\beta = \sqrt{q/\pi\epsilon_s}/V_{th}$, C is a parameter dependent on the trap concentration, ϕ_d is the barrier height for the electron emission from the trap state, ϵ_s is the permittivity and V_{th} is the thermal voltage. The total PF emission current is derived from the current density expression in a similar manner described for FN tunneling current and is expressed as:

$$\begin{aligned} I_{PF} =& K^{'} \Bigg[\left(\frac{K_1}{K_4} - \frac{K_2}{K_4^2} - \frac{2K_3}{K_4^3} \right) \frac{sinh\left(K_4\Delta\psi/2\right)}{\Delta\psi/2} \\ &- \frac{K_3(\Delta\psi/2)}{K_4} sinh\left(\frac{K_4\Delta\psi}{2}\right) \\ &+ \left(\frac{K_2}{K_4} + \frac{2K_3}{K_4^3}\right) cosh\left(\frac{K_4\Delta\psi}{2}\right) \Bigg] \end{aligned} \tag{8}$$

where the variables are reassigned as; $K^{'} = (WLC/K)exp(\alpha + \beta\sqrt{E_m})$, $K_1 = KE_m$, $K_2 = K/d - E_m$, $K_3 = 1/d$, and $K_4 = \beta/(2d\sqrt{E_m})$.

TAT is the other trap-assisted transport mechanism which becomes significant in the vicinity of zero gate bias to compensate the non-zero PF current at this bias. In this process, electrons tunnel from metal to semiconductor through a band of localized traps [9] present in AlGaN layer. The trap-assisted current density is expressed as [15]:

$$J_{TAT} = J_{TAT0}\left[exp\left(\frac{V_g - V_0 - \psi}{\eta_1 V_{th}}\right) - 1\right] \tag{9}$$

where J_{TAT0} is the reverse saturation current density, which is calculated by equating J_{TAT} to J_{PF} at zero gate voltage, η_1 is the ideality factor and V_0 is the voltage used to fit the experimental data close to the origin. We get the TAT current expression by integrating the current density along the channel and is expressed in terms of ψ as:

$$\begin{aligned} I_{TAT} =& C_1 \Bigg[exp\left(\frac{V_g - V_0 - \psi_m}{\eta_1 V_{th}}\right) .\eta_1 V_{th} \Bigg[cosh\left(\frac{\Delta\psi/2}{\eta_1 V_{th}}\right) \\ &- (\eta_1 V_{th} - K)\frac{sinh\left(\Delta\psi/2\eta_1 V_{th}\right)}{\Delta\psi/2}\Bigg] - K \Bigg] \end{aligned} \tag{10}$$

where C_1 is WLJ_{TAT0}/K.

C. Thermionic Emission Current

TE is the dominant mechanism in the forward bias range and the current-voltage characteristics of a Schottky contact is given by [18]:

$$J_{TE} = J_{TE0}\left[exp\left(\frac{V_g - \psi}{\eta_2 V_{th}}\right) - 1\right] \tag{11}$$

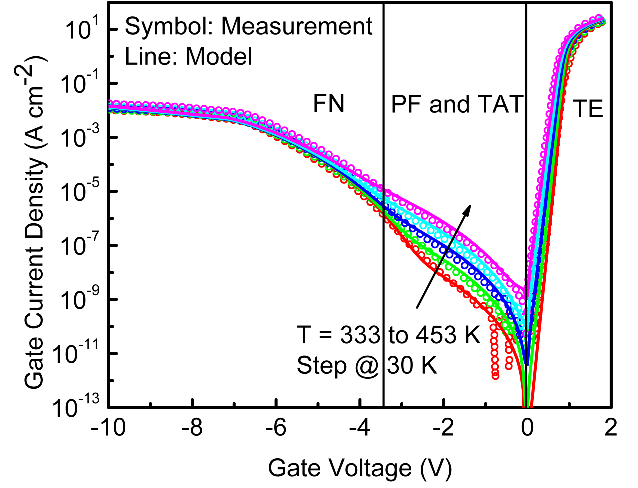

Fig. 3: Experimental gate current density data [8] and model for a wide range of temperature (from 333 to 453 K at a step size of 30 K), showing the three bias regions. Weak temperature dependence in high reverse bias and strong temperature dependence at medium reverse bias clearly distinguish the FN and PF current components for this device (Al mole fraction 33 %); TE plays important role in forward bias region. Impact of the gate-resistance is seen in high forward bias region.

$$J_{TE0} = A^{*}T^{2}exp\left(-\frac{\phi_b}{V_{th}}\right) \tag{12}$$

where J_{TE0} is the reverse saturation current density, A^{*} the effective Richardson's constant, ϕ_b the Schottky barrier height, η_2 the ideality factor. Integrated TE current expression is similar to the TAT current, except the V_0 term. In high forward bias region gate current deviates from the exponential increasing behavior which is modeled by adding a constant gate resistor between intrinsic and extrinsic gate terminal.

III. Results and Discussion

The total gate current for a wide bias range is obtained by adding all the four components described earlier. These components are added separately at source and drain side by considering an appropriate partitioning scheme.

We have validated proposed gate current compact model with measured gate current density vs V_g data [8] of AlGaN/GaN HEMT device with higher Al mole fraction (33 %). From Fig. 3, we can clearly distinguish the FN tunneling current component in high reverse V_g bias region where temperature dependence is less. At low to medium reverse biases, PF emission current dominates. This PF component has a strong temperature dependence, which has been accurately captured through this model. Although the FN tunneling current normally becomes more prominent at low temperature where PF current should not show much effect; but in this case we can see the significant effect of FN tunneling current even above room temperature. In the forward bias region, the TE current and its temperature dependence is well predicted by the model.

To investigate the reverse gate leakage current behavior in high negative V_g (beyond V_{OFF}), we have performed TCAD simulation of a typical AlGaN/GaN HEMT structure and have probed the electric field across the barrier layer which is presented in Fig. 4 (left-Y axis). We can clearly observe that

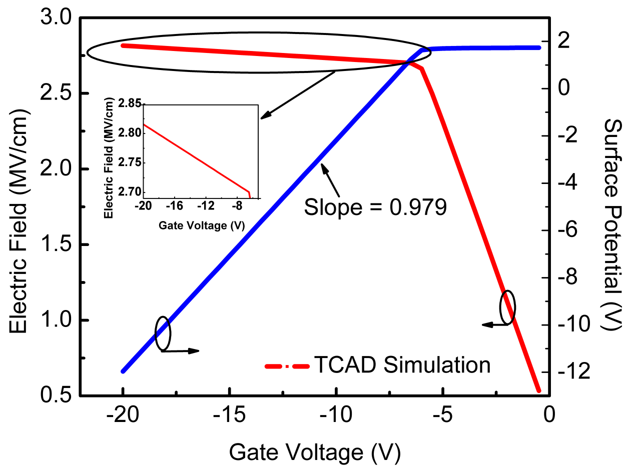

Fig. 4: TCAD simulation result (Silvaco ATLAS) of a typical AlGaN/GaN HEMT structure showing the electric field (left-Y axis) and surface potential (right-Y axis) behavior with reverse gate bias. Inset plot clearly shows that the field does not saturate even in a very high negative gate bias due to the non-unity slope of linearly varying surface potential in this region (beyond V_{OFF}).

the rate of increase of field with V_g changes beyond V_{OFF}, but it does not saturate even when the reverse gate bias is very high. The surface potential plot (Fig. 4, right-Y axis) shows that it varies linearly with V_g beyond V_{OFF} and the slope is less than unity (slope $\approx$ 0.979). This is the reason why electric field continues to increase at a much slower rate with gate voltage in high reverse bias region. The slowly varying non-saturated field in this bias region is sufficient to increase the reverse gate leakage current drastically by FN tunneling mechanism which is clearly visible through the gate current plot in linear scale shown in Fig. 5. Our surface potential calculation used in electric field expression (2) is able to capture this effect which is demonstrated in Fig. 5, showing accurate fitting of reverse gate current (linear scale) up to a high negative bias. In Fig. 6, we show the modeling result of reverse gate current behavior at zero drain current (I_d). Beyond threshold voltage, gate leakage current increases rapidly and to maintain $I_d = 0$ condition, drain voltage starts to increase sharply in the reverse direction. Good agreement between the experimental data and model justifies the overall physics based implementation of the proposed model.

The Verilog-A implemented model is tested with different commercial simulators for a wide temperature and bias ranges, signifies the computational efficiency and robustness of the model due to its tricky formulations.

IV. Conclusion

The reverse and forward gate leakage current is modeled and implemented in physical surface potential based GaN HEMTs compact model. The importance of modeling FN tunneling current is highlighted for the device with higher Al mole fraction in the AlGaN barrier layer. The gate current model is validated with experimental data for wide biases and temperature range. This model is ready to be deployed in a surface-potential-based GaN HEMTs model and is an important step towards developing a complete compact model for these devices.

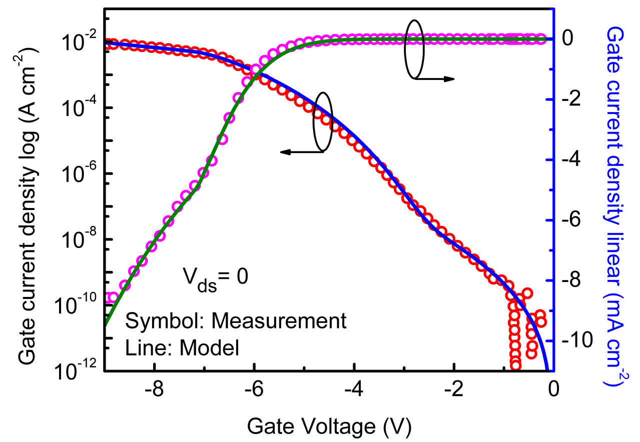

Fig. 5: Measured gate current density data at T=333 K [8] in linear scale clearly shows the non-saturating current beyond V_{OFF} due to the slowly varrying field (FN conduction mechanism). In high negative V_g bias region, model is able to accurately capture this behavior.

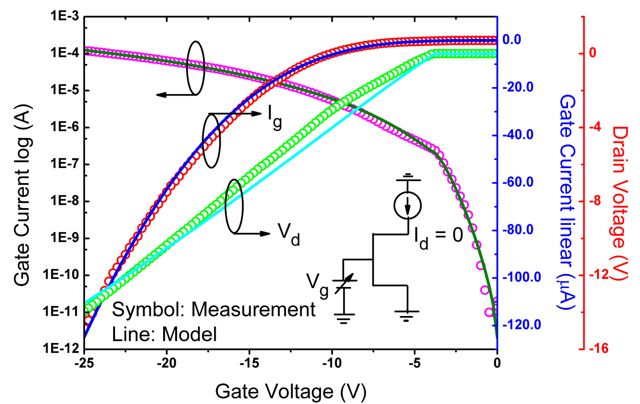

Fig. 6: Gate current measurement at zero drain current condition for the IEMN AlGaN/GaN HEMT (W=50 µm; L_g=200 nm; AlGaN layer thickness=14 nm; Al mole fraction=0.29) showing sharp increase of negative drain voltage beyond V_{OFF} to maintain the measurement condition. Accurate fitting ensures the physical nature of the proposed gate current model.

Acknowledgment

This work was partially supported by DST Fast Track Scheme for Young Scientists, ISRO, and Ramanujan Fellowship. We would like to thank Manchuri Silpa for the fruitful discussions and IEMN for providing experimental data.

References

[1] R. Rupp et al., *IEDM* 2014 pp. 2.3.1-2.3.4.
[2] U. K. Mishra et al., *Proc. IEEE*, vol. 96, no. 2, pp. 287-305, Feb. 2008.
[3] H. Zhang et al., *JAP*, vol. 99, pp. 023703-1-023703-6, Jan. 2006.
[4] D. Yan et al., *APL*, vol. 97, no. 15, pp. 153503-1-153503-3, Oct. 2010.
[5] S. Arulkumaran et al., *APL*, vol. 82, no. 18, pp. 3110-3112, Mar. 2003.
[6] P. D. Ye et al., *APL*, vol. 86, pp. 063501-1-063501-3, Jan. 2005.
[7] N. Ramanan et al., *TED*, vol. 61, no. 6, pp. 2012-2018, June 2014.
[8] S. Turuvekere et al., *TED*, vol. 61, no. 12, pp. 4291-4294, Dec. 2014.
[9] H. R. Mojaver et al., *TED*, vol. 63, no. 4, pp. 1444-1449, April 2016.
[10] S. Khandelwal et al., *TED*, vol.59, no.10, pp.2856-2860, Oct. 2012.
[11] S. Khandelwal et al., *SSE*, vol 76, pp. 60-66, Oct. 2012.
[12] S. Khandelwal et al., *CSICS*, pp. 1-4, 2015.
[13] S. Ghosh et al., *TED*, vol. 62, no. 2, pp. 443-448, Feb. 2015.
[14] A. Dasgupta et. al., *JEDS*, vol. 2, no. 6, pp. 174-178, Nov. 2014.
[15] S. Turuvekere et al., *TED*, vol.60, no.10, pp.3157-3165, Oct. 2013.
[16] S.D. Mertens, *CSICS*, pp. 1-4, 19-22 Oct. 2014.
[17] S. M. Sze, *2nd ed. Wiley*, pp. 402-407, 2001.
[18] E. H. Rhoderick et al., *2nd ed. Oxford*, pp. 98-100, 1988.

View publication stats